Applied Catalysis B: Environmental 130–131 (2013) 178–186

Contents lists available at SciVerse ScienceDirect

Applied Catalysis B: Environmental

journal homepage: www.elsevier.com/locate/apcatb

Hydrothermal fabrication and enhanced photocatalytic activity of hexagram shaped InOOH nanostructures with exposed {0 2 0} facets

Hua Zhao, Wenyan Yin, Mingyuan Zhao, Yuzhe Song, Heqing Yang*

Key Laboratory of Macromolecular Science of Shaanxi Province, School of Materials Science and Engineering, Shaanxi Normal University, Xi'an 710062, China

ARTICLE INFO

Article history:
Received 29 May 2012
Received in revised form 22 October 2012
Accepted 28 October 2012
Available online 9 November 2012

Keywords:
InOOH
Hexagram shaped nanostructures
Exposed {0 2 0} facets
Photocatalytic activity
Rhodamine B

ABSTRACT

Hexagram shaped InOOH nanostructures with exposed {0 2 0} facets were synthesized in large quantities via the hydrothermal reaction of $InCl_3$ with NaAc, ethylene glycol and H_2O system at 180–220 °C for 12 h. The six constituent nanocones of the hexagram shaped nanostructure grew along the directions perpendicular to $(2\,0\,0)/(\bar{2}\,0\,0)$, $(1\,0\,1)/(\bar{1}\,0\,\bar{1})$ and $(\bar{1}\,0\,1)/(1\,0\,\bar{1})$ facets of the orthorhombic InOOH through the oriented attachment process, and the top and bottom surfaces of the hexagrams were dominantly enclosed by the {0 2 0} facets. The {0 2 0} facets were stabilized by ethylene glycol, which was employed to control the growth of InOOH crystals. When the hydrothermal reaction temperature increased, the size of hexagram shaped InOOH nanostructures decreased, their specific surface area and the texture coefficient (TC) of (0 2 0) plane increased, and thus their photocatalytic activity was enhanced. The hexagram shaped InOOH nanostructures obtained at 220 °C showed higher intrinsic photocatalytic activity than Degussa P25 TiO_2 for degradation of rhodamine B. The superior intrinsic photocatalytic activity was attributed to the high percentage of exposed {0 2 0} facets of the hexagram shaped nanostructures.

1. Introduction

Since discovery of water photolysis on a TiO_2 electrode in presence of UV by Fujishima and Honda in 1972 [1], semiconductor photocatalysis has received much attention as a potential solution to the worldwide energy shortage and for counteracting environmental degradation [2]. During the past decades, the photocatalytic activities of TiO_2 [3–5], WO_3 [6,7] ZnO [8,9], In_2O_3 [10,11], α-Fe_2O_3 [12], CdS [13], ZnS [13], ZnSe [14], $NiO_x/In_{1-x}Ni_xTaO_4$ [15], etc. in the degradation of toxic organic pollutants and splitting of water have been widely studied [16]. Recently, Li et al. reported the photocatalytic activity of InOOH nanoparticles with irregular morphologies for the degradation of benzene and rhodamine B (RhB) [17,18]. However, the photocatalytic activities of InOOH with well-defined geometric shapes have never been investigated until now.

As we know, semiconducting nanocrystals with well-defined sizes and geometric shapes display chemical and physical properties that differ from those of the bulk materials and have enormous potentials as fundamental building blocks for nanoscale electronic and photonic devices [19,20]. As for InOOH, an n-type semiconductor with a wide band gap of 3.5 eV, nanofibers [21], nanowires [22], nanorods [23,24], nanotubes [24,25], multipods [26], hollow microspheres [27], urchin-like structures [11], and 3-D architectures [28] have been synthesized via various wet chemical methods, but these InOOH nanostructures are simply employed as precursors for synthesis of In_2O_3 nanocrystals with well-defined geometric shapes, and their crystal structure, physical and chemical properties have hardly been studied. To the best of our knowledge, the photocatalytic activity of single crystalline hexagram shaped InOOH nanostructures have never been reported until now.

Herein, we demonstrate the facile fabrication of hexagram shaped InOOH nanostructures with dominant {0 2 0} surfaces in the $InCl_3$-ethylene glycol (EG)-NaAc-H_2O hydrothermal system. Average size, specific surface area and the texture coefficient (TC) of (0 2 0) plane of the hexagram shaped InOOH nanostructures can be adjusted by changing the hydrothermal reaction temperature. The growth mechanism and photocatalytic activities of the InOOH hexagram in the degradation of RhB were investigated in detail. The as-prepared hexagram shaped InOOH nanostructure with exposed {0 2 0} facets shows higher intrinsic photocatalytic than Degussa P25 TiO_2 for degradation of rhodamine B.

2. Experimental

2.1. Preparation

All reagents used were of analytical grade and were directly used as received without any further purification. 0.510 M aqueous

* Corresponding author.
E-mail address: hqyang@snnu.edu.cn (H. Yang).

0926-3373/$ – see front matter © 2012 Elsevier B.V. All rights reserved.
http://dx.doi.org/10.1016/j.apcatb.2012.10.027

solution of $InCl_3$ was obtained by dissolving 15.000 g of $InCl_3 \cdot 4H_2O$ in 100.0 mL of 0.12 M hydrochloric acid.

The hexagram shaped InOOH nanostructures. In a typical procedure, 0.88 ml of 0.510 M $InCl_3$ aqueous solution, 5.0 mL of water and 0.367 g of $NaAc \cdot 3H_2O$ were put into a beaker of 50 mL capacity, stirred to form a clear solution (pH of about 6). Then 24.0 mL of EG was added into the clear solution under stirring. After 10 min, the mixed solution was transferred into a Teflon-lined autoclave of 50 mL capacity. The autoclave was sealed and heated at 180–220 °C for 12 h. After hydrothermal treatment, the autoclave was cooled down to room temperature naturally. The resulting white products were isolated by centrifugation, washed with water and absolute ethanol, and finally dried in air at room temperature.

2.2. Characterization

The as-prepared products were characterized and analyzed using powder X-ray diffraction (XRD), scanning electron microscopy (SEM), transmission electron microscopy (TEM), and infrared (IR) spectroscopy. The XRD analysis was performed using a Rigaku D/MAX2500VB+ X-ray diffractometer with Cu Kα (λ = 1.541 Å) radiation at 40 kV and 100 mA. Each specimen was scanned at a step size of 0.02° and a scanning speed of 4°/min with diffraction angles varying between 20° and 70°. SEM images were obtained on a FEI Quanta 200 scanning electron microscope at an accelerating voltage of 20 kV. TEM and electron diffraction images were obtained using a JEOL JEM-2100 transmission electron microscope at an accelerating voltage of 200 kV. Samples for TEM were prepared by dispersing InOOH powder on a carbon-coated copper grid. IR spectrum was recorded using a Nicolet Avatar 360E.S.P Fourier transform IR spectrophotometer at room temperature. The specific surface area was measured by nitrogen adsorption/desorption using Brunauer–Emmett–Teller (BET) method on an ASAP 2020 Surface and Porosimetry Analyzer (Micromeritics, USA).

2.3. Evaluation of photocatalytic activity

RhB was selected as model organic compounds to examine the photocatalytic activity of the InOOH hexagram shaped nanostructures. 30.0 mg of the as-prepared photocatalysts was added to 30.0 mL of 2.5×10^{-5} M RhB aqueous solution to get a suspension. The suspension was magnetically stirred for 30 min in the dark to establish an adsorption/desorption equilibrium between the dye and the photocatalyst. Then the mixed solution was irradiated with a 300 W medium-pressure mercury-vapor lamp at a distance of about 8 cm (XPA-7 photochemical reactor, Xujiang Electromechanical Plant, Nanjing, China). At a given irradiation time interval, 5 mL of sample was withdrawn from the test tube for analysis. Sample solutions were obtained by centrifugation, and their absorption spectra were measured by on a Hitachi U-3900 spectrophotometer using deionized water as reference. For comparison, the photocatalytic activities of commercial TiO_2 (Degussa P25) were also tested under the same reaction conditions and with the equal catalyst weight as that employed for InOOH.

3. Results and discussion

3.1. Morphology and crystal structure

The morphology and crystal structure of the as-synthesized samples were investigated by SEM and XRD. Fig. 1a and b shows the typical SEM images of the sample prepared at 180 °C for 12 h. It can be observed that the sample consists almost entirely of hexagram-shaped nanostructures with six symmetric arms extending radically from the center. The average size was

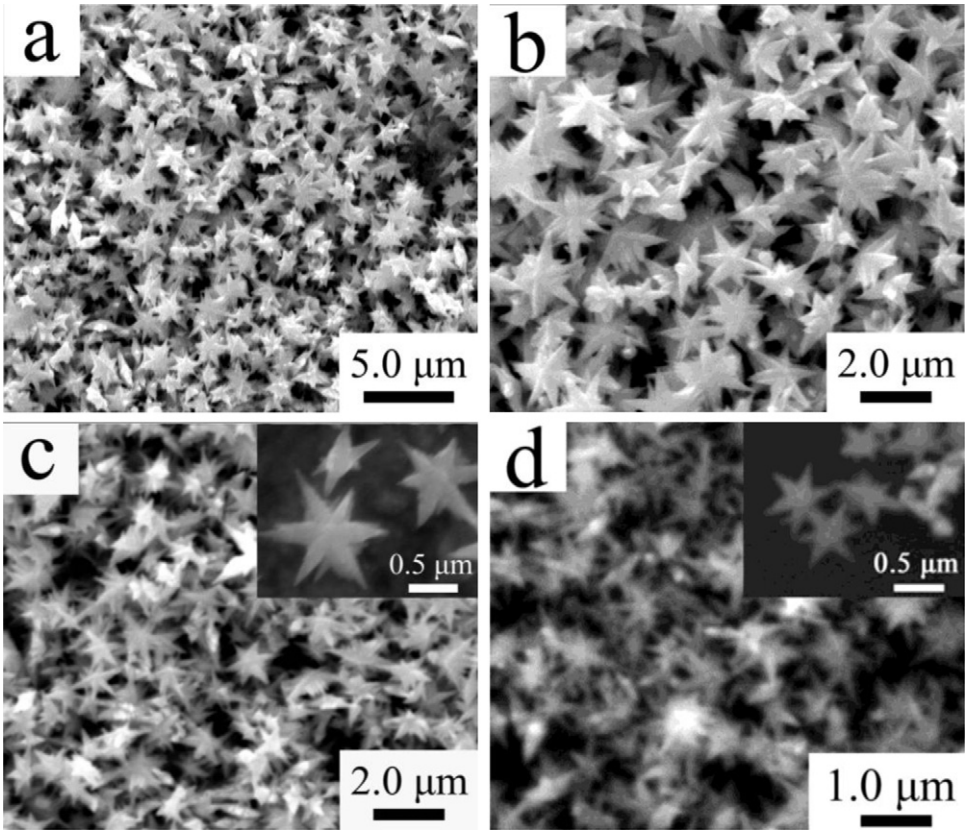

Fig. 1. SEM images of hexagram shaped InOOH nanostructures prepared at 180 °C (a) and (b), 200 °C (c) and 220 °C (d) for 12 h.

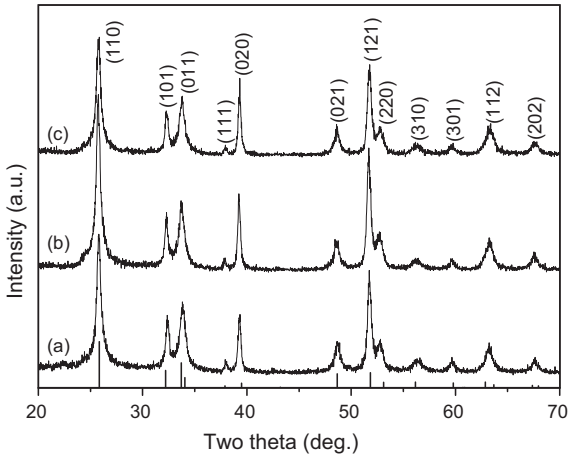

Fig. 2. XRD patterns of hexagram shaped InOOH nanostructures prepared at 180 (a), 200 (b) and 220 °C (c) for 12 h. The stick pattern is the standard XRD pattern of orthorhombic InOOH powders with Cu Kα radiation (JCPDS card no. 71-2283).

calculated to be about 1.6 μm from 100 measured particles. Fig. 1c and d show the representative SEM images of the samples synthesized at 200 and 220 °C for 12 h, respectively. As it can be seen, the both samples are also composed mainly of hexagram-shaped particles, and their average sizes are about 1.1 μm and 0.7 μm, respectively. The above results suggest that size-controlled synthesis of hexagram-shaped nanostructures can be achieved by changing the hydrothermal reaction temperature. Fig. 2 shows the XRD patterns of the hexagram-shaped structures prepared in the hydrothermal system at 180, 200 and 220 °C for 12 h. All the reflections of the XRD patterns could be perfectly indexed to pure orthorhombic InOOH (JCPDS card no. 71-2283), suggesting that the hexagram-shaped nanostructures are InOOH with an orthorhombic structure. Moreover, the higher intensity ratios of (0 2 0) to other diffraction peaks in comparison with those in the corresponding standard pattern of orthorhombic InOOH are observed, which suggests that the InOOH hexagrams are primarily dominated by (0 2 0) facets.

Further structural details of the as-synthesized hexagram shaped InOOH nanostructures were studied by TEM observations and SAED patterns. Fig. 3a presents representative TEM images of individual hexagram shaped InOOH nanostructures synthesized at 220 °C for 12 h. The TEM image further corroborates the hexagram geometrical shape of the InOOH nanostructures. The hexagram shaped nanostructure consists of six symmetric nanocones with lengths of 200–400 nm, and the angles between the neighboring nanocones are measured to be 58° or 64°. The tip diameter of the nanocones is in the range of 20–40 nm. A higher magnification TEM image from circle in (a) is shown in Fig. 3b, which indicates that the hexagram shaped InOOH nanostructures have rough surfaces. Fig. 3c and d show selected area electron diffraction (SAED) pattern and high-resolution TEM (HRTEM) image from circle in (b), respectively. The SAED pattern can be indexed to [0 2 0] zone axis of orthorhombic phase InOOH. The lattice spacings of 0.26 and 0.28 nm can be observed clearly from the HRTEM image, which correspond to (2 0 0) and (1 0 1) facets, respectively. The SAED and HRTEM results indicate that the six constituent nanocones of the hexagram shaped nanostructure grow along the directions perpendicular to (2 0 0), $(\bar{2}\,0\,0)$, (1 0 1), $(\bar{1}\,0\,\bar{1})$, $(\bar{1}\,0\,1)$ and $(1\,0\,\bar{1})$ facets of the orthorhombic InOOH and are dominantly enclosed by {0 2 0} top and bottom surfaces.

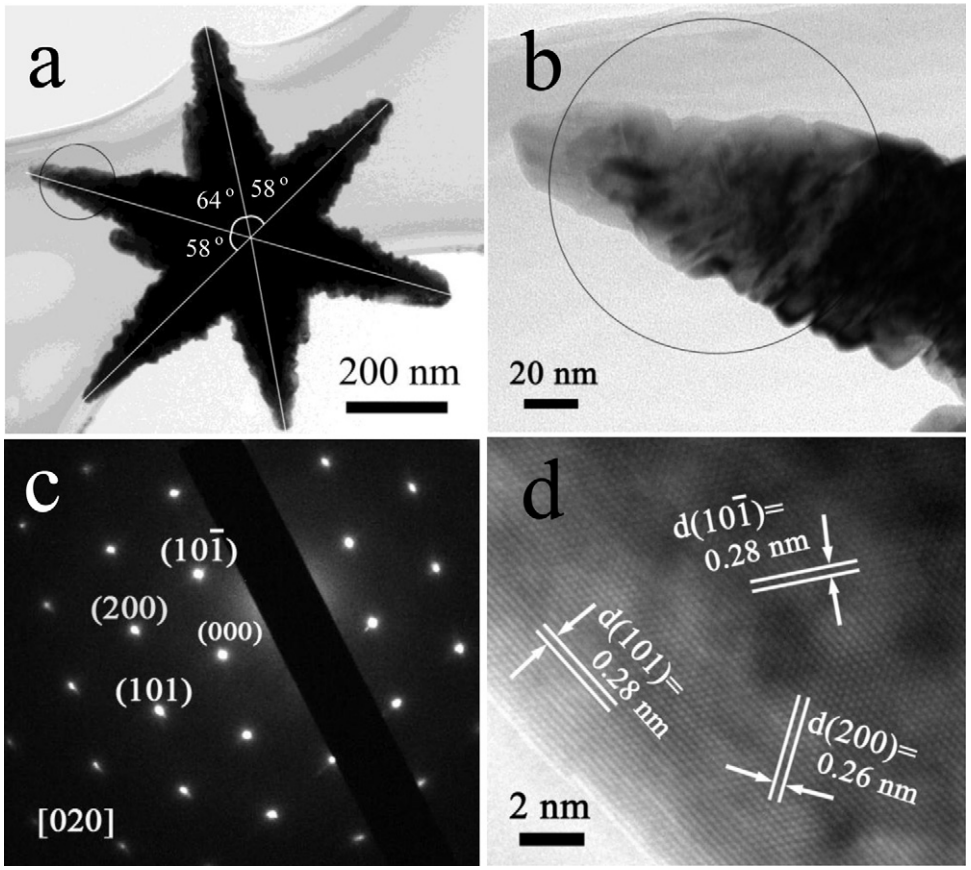

Fig. 3. (a) TEM images of the InOOH hexagrams synthesized at 220 °C for 12 h. (b) High magnification TEM image from circle in (a). (c) and (d) SAED pattern and HRTEM image from circle in (b), respectively.

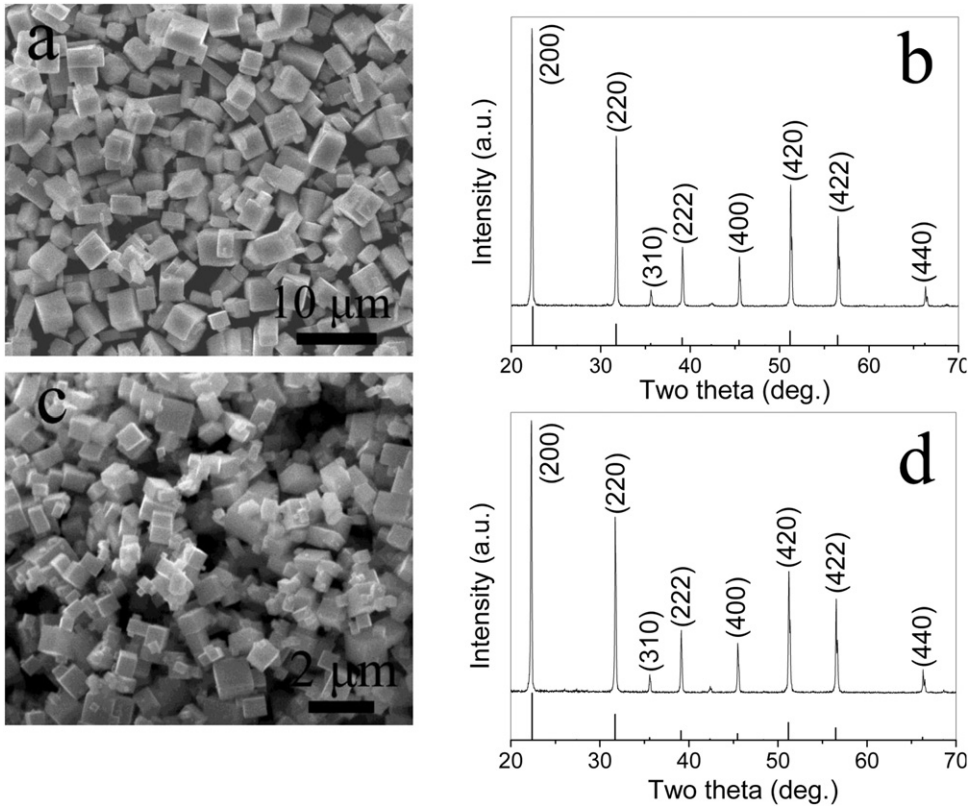

Fig. 4. (a) SEM image and (b) XRD pattern of the products obtained by using water instead of EG. (c) SEM image and (d) XRD pattern of the products obtained by using ethanol instead of EG. The stick patterns in (b) and (d) are the standard XRD pattern of cubic $In(OH)_3$ powders with Cu Kα radiation (JCPDS card no. 76-1464).

3.2. The effects of ethylene glycol (EG) and sodium acetate (NaAc) on the structureand morphology of the hexagram shaped InOOH nanostructure

To understand the role of EG in the formation of the hexagram shaped InOOH nanostructure, the same dosage of deionized water and ethanol were used instead of 24 mL EG, respectively. The products obtained via the same experimental procedure at 180 °C for 12 h was characterized with SEM and XRD, and the results are shown in Fig. 4. As shown in Fig. 4, when 24 mL EG was replaced by the same dosage of deionized water the as-obtained products are composed of cubelike particles instead of hexagram shaped nanostructures (Fig. 4a). The edge lengths are in the range of 1.3–5.6 μm. The corresponding XRD pattern shown in Fig. 4b indicates that these cubelike particles are pure body-centered cubic (bcc) $In(OH)_3$ instead of the orthorhombic InOOH. The products obtained by employing 24 mL of ethanol are also composed of cubelike $In(OH)_3$ particles with the edge lengths of 0.27–1.2 μm and the bcc structures instead of orthorhombic InOOH hexagram shaped structures (Fig. 4c and d).The results reveal that EG is indispensable for the formation of the orthorhombic InOOH hexagram shaped structure.

Moreover, IR spectrum of the hexagram shaped InOOH nanostructures prepared via the hydrothermal reaction of $InCl_3$ with EG, H_2O and NaAc at 180 °C for 12 h was measured, and the result is shown in Fig. 5. In the IR spectrum, the two broad bands at 3438 and 1638 cm^{-1} are attributed to the O—H stretching and bending vibrations [31], respectively, which might come from O—H of InOOH. Two bands at 2918 and 2852 cm^{-1} correspond to $-CH_2$ asymmetric and symmetric stretching modes, respectively [29,30]. The bands at 1385 cm^{-1} is attributed to combinatorial effect of bending the —C—O—H and wagging CH_2 vibrations [29,30]. The absorption band at 1159 cm^{-1} can be assigned to C—O stretching vibration [30] and the peaks at 400–500 cm^{-1} are the In–O feature modes [22]. The IR spectrum suggests that EGs may be adsorbed on the surfaces of the hexagram shaped InOOH nanostructures formed in the hydrothermal system [31].

To investigate the effect of NaAc on the formation of hexagram shaped InOOH nanostructures, the 0. 367 g (2.7 mmol) of $NaAc{\cdot}3H_2O$ was replaced by the same molar amount of NaCl (0.158 g), and the pH value of the solution are adjusted to be the same as that of the mixed solution of $InCl_3$ and NaAc. The products obtained via the same experimental procedure at 180 °C for 12 h was characterized with SEM and XRD, and the results are

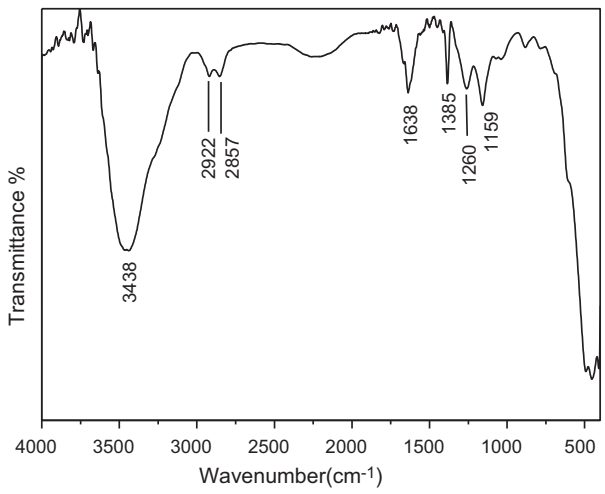

Fig. 5. Infrared (IR) spectrum of the hexagram shaped InOOH nanostructures prepared via the hydrothermal reaction of $InCl_3$ with H_2O in the presence of NaAc and EG at 180 °C for 12 h.

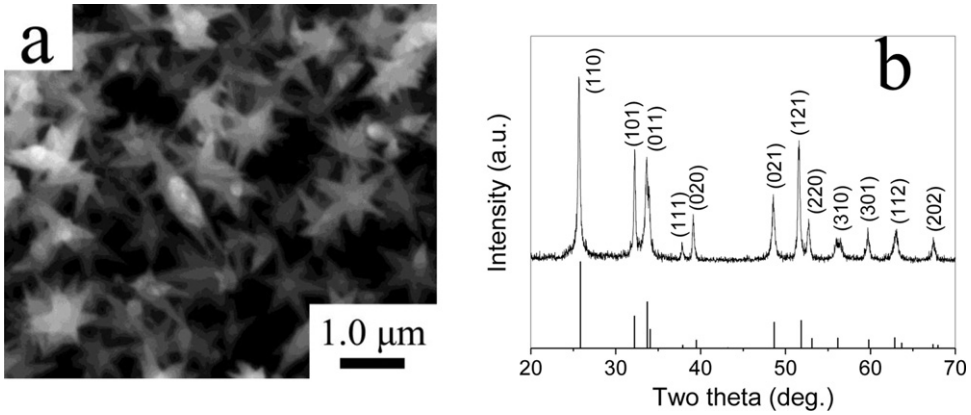

Fig. 6. (a) SEM images and (b) XRD patterns of the products obtained via the hydrothermal reaction of $InCl_3$ with H_2O and EG in the presence of NaCl at 180 °C for 12 h. The stick pattern in (b) is the standard XRD pattern of orthorhombic InOOH powders with Cu Kα radiation (JCPDS card no. 71-2283).

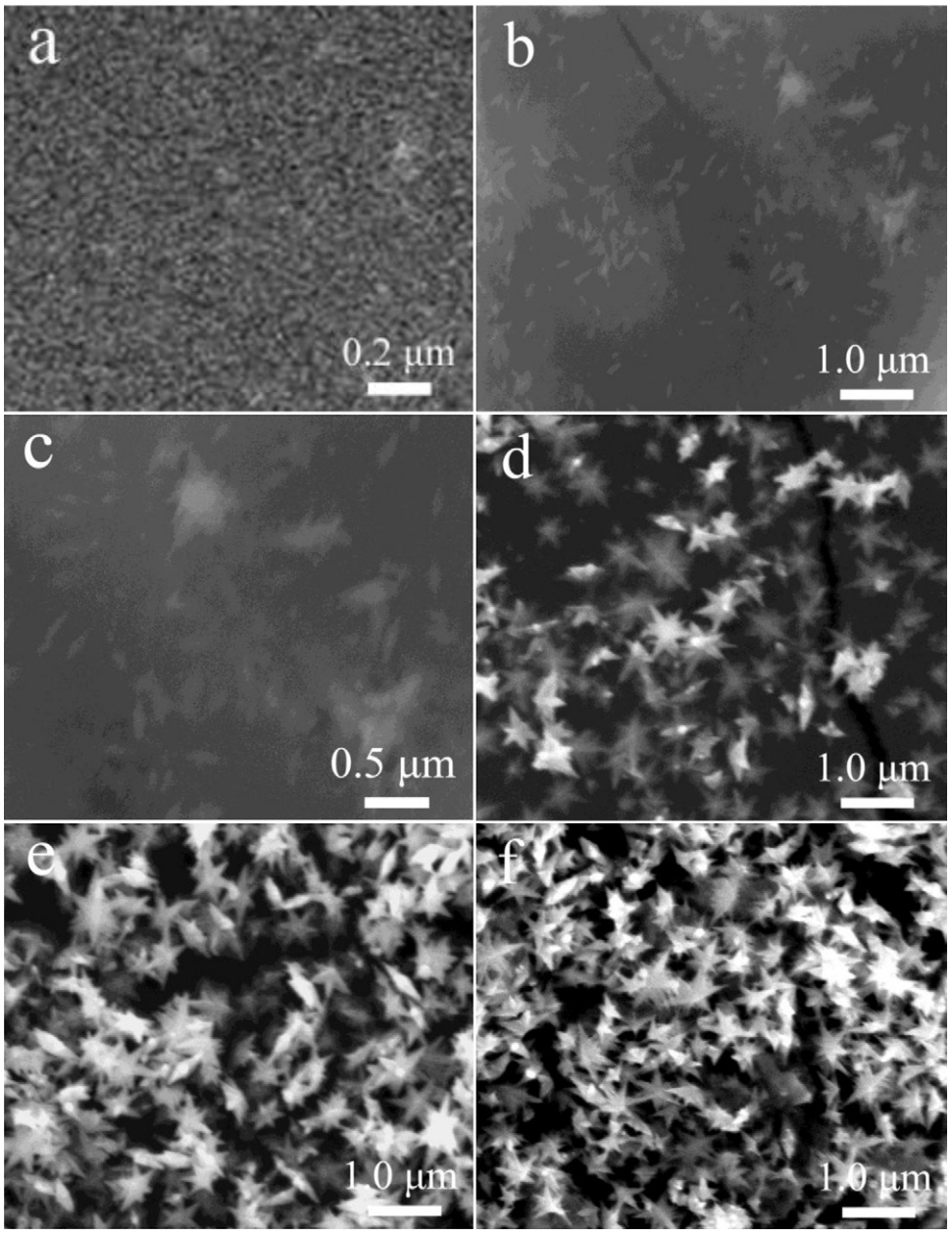

Fig. 7. SEM images of the products prepared via the hydrothermal reaction at 220 °C for 120 min (a), 140 min (b) and (c), 150 min (d), 160 min (e), and 170 min (f).

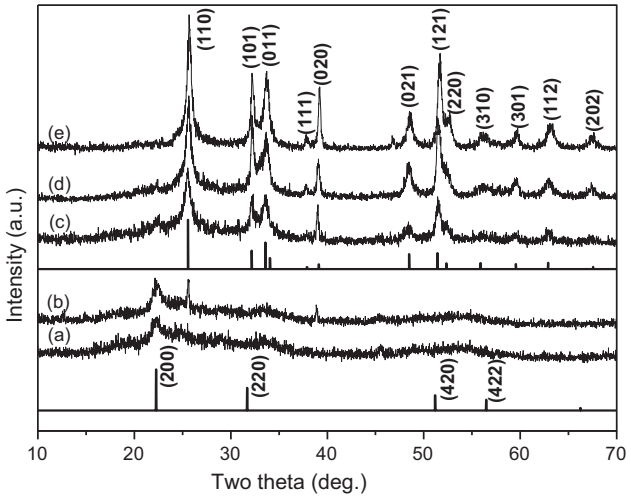

Fig. 8. XRD patterns of the products prepared via the hydrothermal reaction at 220 °C for 120 min (a), 140 min (b), 150 min (c), 160 min (d) and 170 min (e). The upper and lower stick patterns are the standard XRD patterns of orthorhombic InOOH (JCPDS card no. 71-2283) and cubic In(OH)3 (JCPDS card no. 76-1464), respectively.

shown in Fig. 6. The SEM images and XRD patterns reveal that the products obtained in absence of NaAc consist of the hexagram shaped InOOH structures. Therefore, it is reasonable to conclude that the NaAc neutralizes HCl in $InCl_3$ solution, and provides an appropriate pH value for the formation and growth of the InOOH hexagram shaped nanostructures.

3.3. Growth process of hexagram shaped InOOH nanostructures

To investigate the formation process of the hexagram shaped InOOH nanostructures, time-dependent experiments at 220 °C were carried out and the resultant products were analyzed by SEM and XRD. Fig. 7 displays SEM images of the samples prepared at various reaction stages. The SEM image in Fig. 7a shows the as-obtained products at 220 °C for 120 min consist of a large quantity of nanoparticles with the size of about 20 nm. As the reaction time was prolonged to 140 min, some shuttle-like and multipodal structures were found among the nanoparticle agglomerates (Fig. 7b and c). When the reaction time was further increased to 150–170 min, the as-obtained products were mainly composed of hexagram shaped structures. Their sizes increased slightly with increasing the reaction time, however, the yields increased obviously (Fig. 7d–f). Corresponding XRD patterns of the samples obtained for different reaction times at 220 °C are displayed in Fig. 8. The XRD indicates that the nanoparticle agglomerates obtained at 220 °C for 120 min may be $In(OH)_3$ with a cubic structure. The nanoparticle agglomerates containing shuttle-like and multipodal structures obtained at 220 °C for 140 min may be a mixture of cubic $In(OH)_3$ and orthorhombic InOOH. When the reaction time is increased to 150–180 min, the as-obtained hexagram shaped structures are phase-pure orthorhombic InOOH. Furthermore, intensities of the InOOH diffraction peaks increase with the reaction time, and thus the crystallinity of the hexagram shaped InOOH nanostructures is improved.

3.4. The formation mechanism for the InOOH hexagram shaped nanostructures

In the hydrothermal reaction, $InCl_3$ reacted with H_2O to form $In(OH)_3$, which was partly decomposed to form InOOH. The chemical reactions are formulated as follows:

$$InCl_3 + H_2O \rightarrow In(OH)_3 + HCl \quad (1)$$

$$In(OH)_3 \rightarrow InOOH + H_2O \quad (2)$$

On the basis of the investigations described above, a possible mechanism to form InOOH hexagram shaped nanostructures was proposed and schematically shown in Fig. 9. Initially, $In(OH)_3$ monomers are formed via the reaction (1). In the presence of EG, after nucleation the $In(OH)_3$ monomers grow into $In(OH)_3$ nanocrystallites stabilized by EG molecules (step a). The InOOH nanocrystallites stabilized by EG molecules are formed by the dehydration of these $In(OH)_3$ nanocrystallites with increasing the reaction time. These InOOH nanocrystals grew into hexagram shaped nanostructures via an oriented attachment process [32] (step b). Size of the hexagram shaped structures increases continuously with an increase on the reaction time (step c–d). The crystal structure of orthorhombic InOOH can be described as a packing of indium-oxygen octahedra. Chains of octahedra sharing edges are stacked along the [0 0 1] direction. The parallel chains are interlinked by sharing the corners of the octahedra [33]. Fig. 10a shows the systems of octahedra and hydrogen bonds joining them together. As we know, the growth of certain surfaces can be impeded by using additives that preferentially adsorb to specific crystal faces. The distance between both oxygen atoms within the indium–oxygen octahedron of orthorhombic InOOH {0 2 0} facets is 0.279 nm [34]. In EG ($C_2H_6O_2$) molecule, the distance between the two oxygen atoms is about 0.282 nm [35]. Therefore, in the hydrothermal system, EG may serve as a ligand to In (III), and adsorbs selectively on the (0 2 0) prismatic faces of the InOOH crystalline nuclei. The most likely structure is described in Fig. 10b. The presence of EG impedes the growth of the (0 2 0) surface of InOOH, and thus the InOOH hexagram like structure are primarily dominated

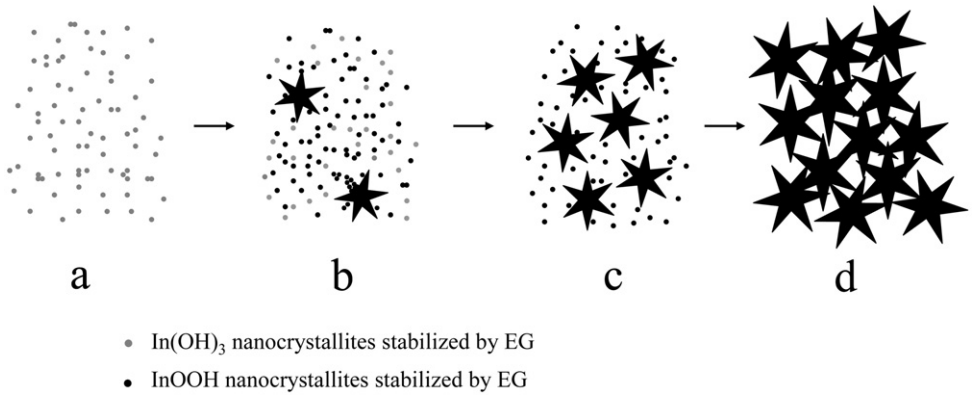

Fig. 9. Schematic illustration of the formation process of the InOOH hexagram shaped superstructures.

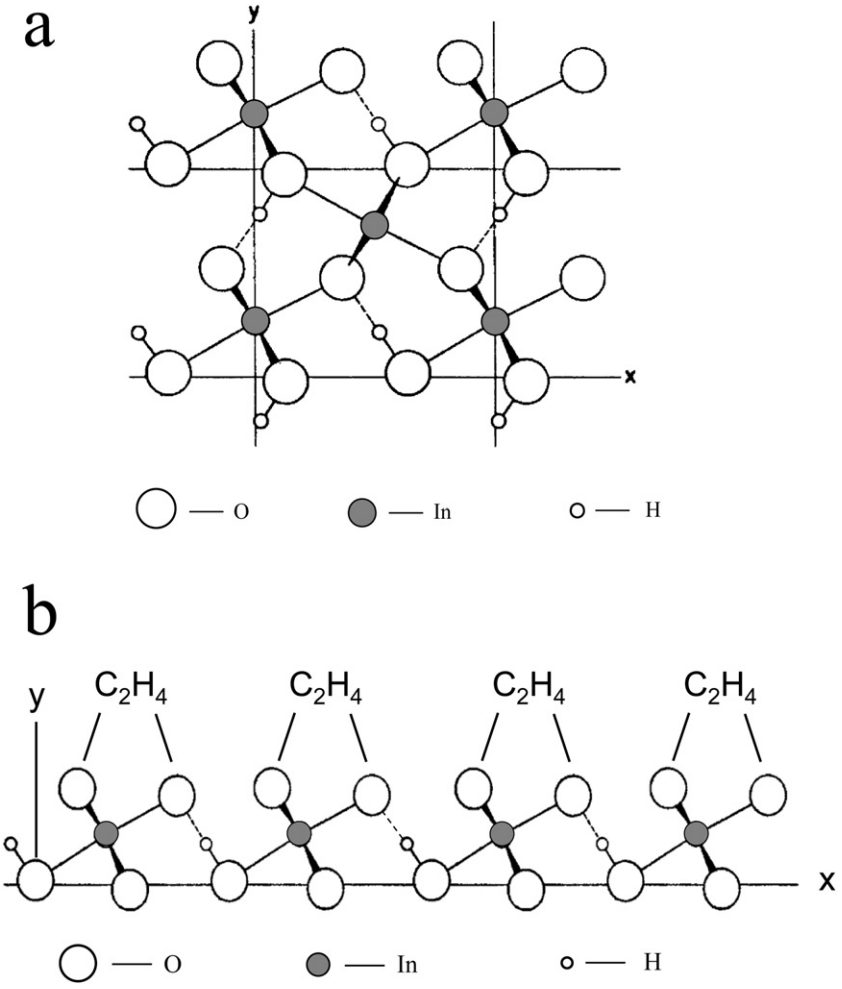

Fig. 10. (a) Projection in the [0 0 1] direction of five octahedra in the indium oxide hydroxide structure. (b) The most likely structure of EG adsorbed selectively on the (0 2 0) prismatic faces.

by (0 2 0) facets. Among crystal facets of InOOH perpendicular to (0 2 0) surface, (2 0 0)/($\bar{2}$ 0 0), (1 0 1)/(1 0 $\bar{1}$) and ($\bar{1}$ 0 1)/(1 0 $\bar{1}$) facets may have relatively higher surface energy, and thus InOOH nanocrystals grew into hexagram shaped nanostructures via an oriented attachment process along six directions perpendicular to the (2 0 0)/($\bar{2}$ 0 0), (1 0 1)/(1 0 $\bar{1}$) and ($\bar{1}$ 0 1)/(1 0 $\bar{1}$) facets. In addition, it is well known that the final size of crystallites usually depends on their nucleation and growth rates. During the formation of hexagram shaped InOOH structures via the oriented attachment, when the hydrothermal system temperature is increased, the higher heating temperature will speed up the nucleation reaction, and induce the formation of more and smaller nuclei [36]. Therefore, the average size of hexagram shaped InOOH structures decreases with an increase on the hydrothermal reaction temperature.

3.5. Photocatalytic activity

To demonstrate the potential applicability in photocatalysis of the as-obtained hexagram shaped InOOH nanostructures, we investigated their photocatalytic activity by choosing photocatalytic degradation of rhodamine B (RhB) as reference. The hexagram shaped InOOH nanostructures synthesized at 220, 200 and 180 °C for 12 h are denoted as catalyst 1, 2, and 3, respectively. Before evaluation of the photocatalytic activity, adsorption capacity of the as-prepared InOOH samples and commercial TiO_2 (P25) for RhB was studied, and the results are shown in Fig. 11. Fig. 11 shows the kinetics of RhB adsorption on the catalysts 1, 2 and 3 as well as P25. The C_0 and C represent the concentration of RhB at initial and any time, respectively. For catalysts 1, 2 and 3 as well as P25, after 30 min, the value of C/C_0 is 0.940, 0.947, 0.940 and 0.957, respectively and hardly decreased with an increase on the time, which indicates an adsorption/desorption equilibrium between the dye and the photocatalysts is achieved within 30 min. Therefore, the suspension containing the dye and catalysts was stirred for

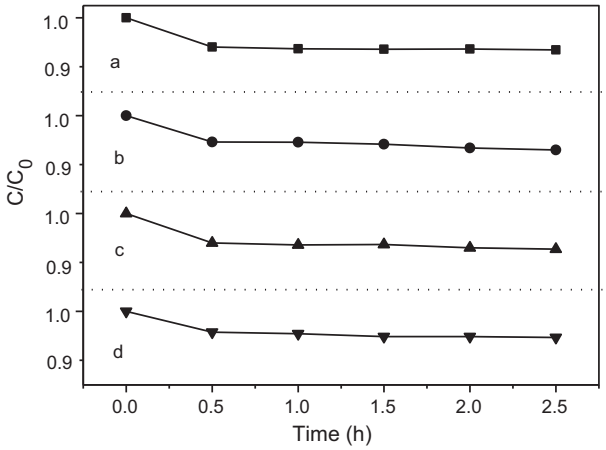

Fig. 11. Adsorption kinetics of RhB on catalyst 1 (a), 2 (b), 3 (c) and P25 (d).

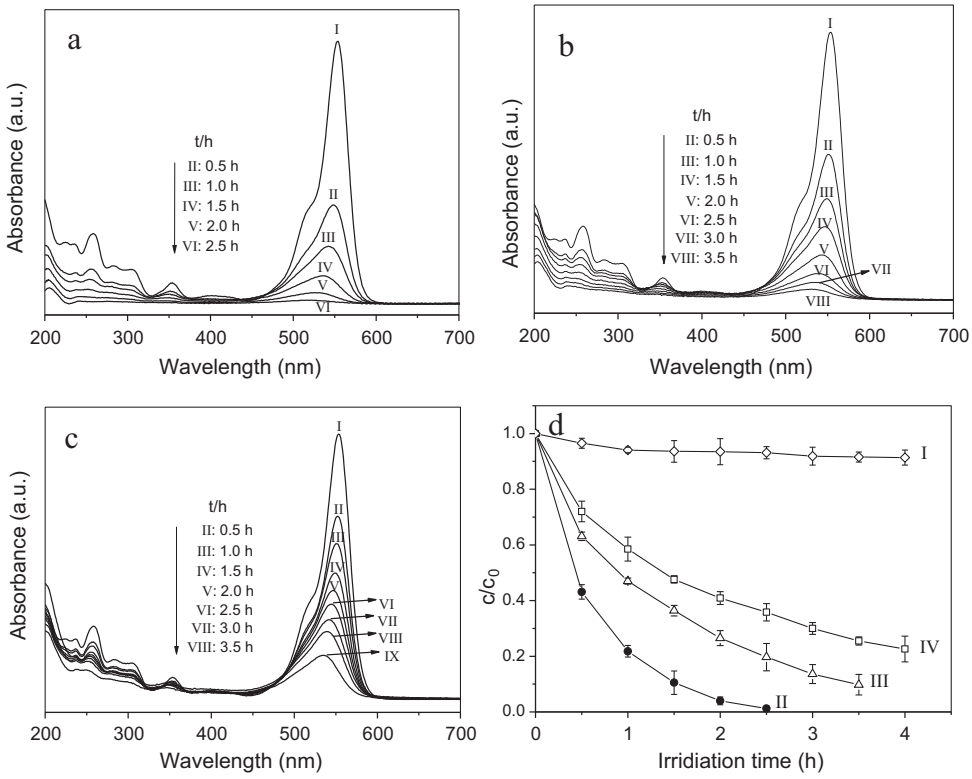

Fig. 12. (a–c) Temporal absorption spectra of RhB solution during the photocatalytic degradation process over catalyst 1 (a), 2 (b) and 3 (c). (d) Photodegradation of the RhB solutions without catalyst (I), over catalysts 1 (II), 2 (III) and 3 (IV) under mercury lamp irradiation, Error bars represent 95% confidence interval with triplicate runs.

30 min in the dark before the mercury lamp irradiation to establish an adsorption/desorption equilibrium between the dye and the photocatalyst.

Fig. 12a–c shows the temporal absorption spectra of RhB solution during the photocatalytic degradation process over catalyst 1 (a), 2 (b) and 3 (c), respectively. RhB shows a maximum absorption band at 553.0 nm (curve I in Fig. 12a–c). In the presence of catalysts 1, 2 and 3, the absorption intensity of the peak is reduced by about 63, 46, and 31%, respectively, after mercury lamp irradiation for 0.5 h. The absorption peaks diminished gradually as the irradiation time was extended, which implies the destruction of the dye chromogen. Since no new absorption peak was observed, the RhB has been decomposed. Fig. 12d shows the decomposition of RhB in solution over catalysts 1, 2, and 3 under mercury lamp irradiation as a function of time. As the irradiation time increases, the decomposition of the RhB progresses relaxedly without hexagram shaped InOOH nanostructures (catalyst) under mercury lamp irradiation. However, the RhB decomposition over the catalysts progresses fleetly and the rate of the RhB decomposition over catalyst 1 is faster than that over catalysts 2 and 3. The results implied that the hexagram shaped InOOH nanostructures are effective photocatalysts for the degradation of RhB, and its photocatalytic activity is enhanced with reducing its size. The fittings of ln (C_0/C) plot vs. time over P25, catalysts 1, 2 and 3 are shown in Fig. 13a. The photodegradation of RhB catalyzed by the four kinds of catalysts fits pseudo first-order reaction. i.e. ln (C_0/C) = Kt, K is the apparent rate constant of the degradation. In our experiment, K is found to be 1.96 ± 0.10, 1.69 ± 0.10, 0.64 ± 0.015 and $0.37 \pm 0.015\ h^{-1}$, over P25, catalysts 1, 2 and 3, respectively. The photocatalytic activity of catalyst 1 is higher than that of catalysts 2 and 3, and lower than that of P25. It is generally accepted that the catalytic process is mainly related to the adsorption and desorption of molecules on the surface of the catalyst. The Brunauer–Emmett–Teller (BET) surface area of Degussa P25, catalysts 1, 2 and 3 was measured to be 55.2, 35.8, 30.3 and 24.9 $m^2\ g^{-1}$, respectively. The apparent rate constant of the degradation per unit surface area of the four kinds of catalysts, as for the basis for the comparison, is examined in this work. The normalized K value (k) of catalyst 1 is higher than that of Degussa P25 TiO_2, catalysts 2 and 3, as seen in Fig. 13b. The results clearly demonstrate that the photocatalytic activity of the as-prepared hexagram shaped InOOH nanostructures is enhanced by increasing hydrothermal reaction temperature, and the as-prepared samples at 220 °C for 12 h (catalyst 1) possesses higher intrinsic photocatalytic activity than Degussa P25 TiO_2.

Excellent photocatalytic activity of InOOH may be attributed to its peculiar electronic structure as a wide band gap p-block semiconductor [17]. The dispersive conduction band of InOOH promotes the mobility of the photogenerated electrons and enhances the charge separation. Besides this, the wide band gap endows the photogenerated holes and electrons with strong redox ability and long lifetime, and thus InOOH show excellent photocatalytic activity for degradation of RhB. In addition, the XRD and TEM analyses (Figs. 2 and 3) indicate that the InOOH hexagram shaped InOOH nanostructures are primarily dominated by (0 2 0) facets. The texture coefficient (TC) of (0 2 0) plane is defined as [37]

$$\mathrm{TC}(0\ 2\ 0) = \frac{I(0\,2\,0)}{I_0(0\,2\,0)} \left\{ \frac{1}{n} \sum \frac{I(h\ \ k\ \ l)}{I_0(h\ \ k\ \ l)} \right\}^{-1} \quad (3)$$

where $I(h\ k\ l)$ are measured intensities of ($h\ k\ l$) reflection, $I_0(h\ k\ l)$ are powder diffraction intensities of orthorhombic InOOH according to the JCPDS card no. 71-2283, and n is the number of diffraction peaks used in the calculation. For materials with random crystallographic orientations, e.g. powders, the texture coefficient of any ($h\ k\ l$) reflection should be 1. TC value of (0 2 0) diffraction peaks for catalysts 1, 2 and 3 is 3.5, 3.1 and 2.5, respectively. The value of TC(0 2 0) for the as-synthesized InOOH hexagram shaped InOOH nanostructures increases with an increase on the hydrothermal reaction temperature. The (0 2 0) surfaces may be high-energy

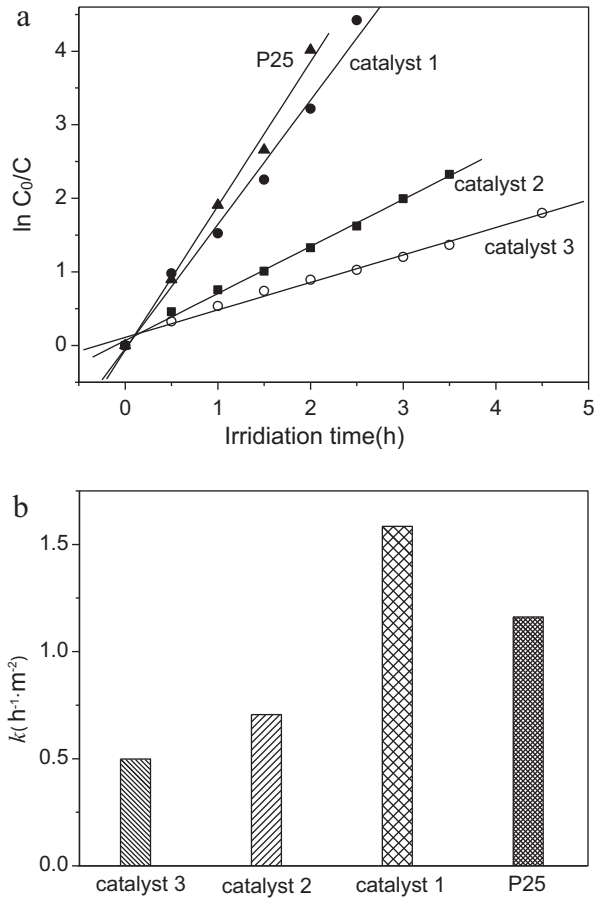

Fig. 13. (a) The fitting of ln (C_0/C) plot vs. time over P25, catalyst 1, catalyst 2 and catalyst 3. (b) Normalized apparent rate constant of the degradation per unit surface area (k) over P25, catalysts 1, 2 and 3.

facets, like the {0 0 1} facets for anatase TiO_2 [38], which possesses higher catalytic activity, and thus catalyst 1 shows higher intrinsic photocatalytic activity than catalysts 2, 3 and Degussa P25. Moreover, the as-obtained hexagram shaped InOOH nanostructures at 220 °C (catalyst 1) have higher specific surface area than that at 200 and 180 °C (catalyst 2 and 3). The high specific surface area can provide more reactive adsorption/desorption sites for photo catalytic reactions, and thus photocatalytic activity of the hexagram shaped InOOH nanoparticles was enhanced via increasing the hydrothermal reaction temperature.

4. Conclusions

In summary, we have developed a facile hydrothermal method to large-scale synthesis of hexagram shaped InOOH nanostructures with exposed {0 2 0} facets. The hexagram shaped InOOH nanostructures was formed via the oriented attachment of EG-stabilized InOOH nano-crystallites. The texture coefficient (TC) of (0 2 0) plane, specific surface area of the as-prepared hexagram shaped InOOH nanostructures increase with increasing the hydrothermal reaction temperature, and thus the photocatalytic activity is enhanced. The hexagram shaped InOOH nanostructures obtained at 220 °C show higher intrinsic photocatalytic activity than Degussa P25 TiO_2 for degradation of rhodamine B, which are expected to be a promising candidate for catalyst applied in pollutant treatment.

Acknowledgements

This work was supported by the National Natural Science Foundation of China (Grant No. 21073116), the Natural Science Foundation of Shaanxi Province (Grant No. 2010JM2011) and the Fundamental Research Funds for the Central Universities (Grant No. GK201101004). We thank Prof. Guang Yang, Dr. Lu Lu from Xi'an Jiaotong University and Prof. Yun Liu form Australian National University for their help in the TEM and SAED measurements.

References

[1] A. Fujishima, K. Honda, Nature 138 (1972) 37–38.
[2] M.R. Hoffman, S.T. Martin, W.Y. Choi, D.W. Bahnemann, Chemical Reviews 95 (1995) 69–96, A.
[3] H. Kim, W. Choi, Applied Catalysis B 69 (2007) 127–132.
[4] P. Periyat, S.C. Pillai, D.E. McCormack, J. Colreavy, S.J. Hinder, Journal of Physical Chemistry C 112 (2008) 7644–7652.
[5] H.G. Yang, G. Liu, S.Z. Qiao, C.H. Sun, Y.G. Jin, S.C. Smith, J. Zou, H.M. Cheng, G.Q. Lu, Journal of American Chemical Society 131 (2009) 4078–4083.
[6] H. Reiche, W.W. Dunn, A.J. Bard, Journal of Physical Chemistry C 83 (1979) 2248–2251.
[7] J.W. Kim, C.W. Lee, W.Y. Choi, Environmental Science and Technology 44 (2010) 6849–6854.
[8] C. Hariharan, Applied Catalysis A 304 (2006) 55–61.
[9] Y.L. Lai, M. Meng, Y.F. Yu, X.T. Wang, T. Ding, Applied Catalysis B 105 (2011) 335–345.
[10] B.X. Li, Y. Xie, M. Jing, G.X. Rong, Y.C. Tang, G.Z. Zhang, Langmuir 22 (2006) 9380–9385.
[11] L.Y. Chen, Y. Liang, Z.D. Zhang, European Journal of Inorganic Chemistry (2009) 903–909.
[12] X.L. Xie, H.Q. Yang, F.H. Zhang, L. Li, J.H. Ma, H. Jiao, J.Y. Zhang, Journal of Alloys and Compounds 477 (2009) 90–99.
[13] A. Kudo, Y. Miseki, Chemical Society Reviews 38 (2009) 253–278.
[14] L.H. Zhang, H.Q. Yang, J. Yu, F.H. Shao, L. Li, F.H. Zhang, H. Zhao, Journal of Physical Chemistry C 113 (2009) 5434–5443.
[15] Z.G. Zou, J.H. Ye, K. Sayama, H. Arakawa, Nature 414 (2001) 625–627.
[16] H. Tong, S.X. Ouyang, Y.P. Bi, N. Umezawa, M. Oshikiri, J.H. Ye, Advanced Materials 24 (2011) 229–251.
[17] Z.H. Li, Z.P. Xie, Y.F. Zhang, L. Wu, X.X. Wang, X.Z. Fu, Journal of Physical Chemistry C 111 (2007) 18348–18352.
[18] X. Chen, P.-Y. Lin, X.-C. Shi, Z.-L. Zhang, Z.-P. Xie, Z.-H. Li, Chinese Journal of Inorganic Chemistry 25 (11) (2009) 1917–1921.
[19] X.F. Duan, Y. Huang, Y. Cui, J. Wang, C.M. Lieber, Nature 409 (2001) 66–69.
[20] B.Z. Tian, T.J. Kempa, C.M. Lieber, Chemical Society Reviews 38 (2009) 16–24.
[21] D.B. Yu, S.-H. Yu, S.Y. Zhang, J. Zuo, D.B. Wang, Y.T. Qian, Advanced Functional Materials 13 (2003) 497–501.
[22] X.X. Xu, X. Wang, Inorganic Chemistry 48 (2009) 3890–3895.
[23] J.Q. Xu, Y.P. Chen, Q.Y. Pan, Q. Xiang, Z.X. Cheng, X.W. Dong, Nanotechnology 18 (2007), 115615.(1–7).
[24] L.-Y. Chen, Z.-X. Wang, Z.-D. Zhang, New Journal of Chemistry 33 (2009) 1109–1115.
[25] C.L. Chen, D.R. Chen, X.L. Jiao, C.Q. Wang, Chemical Communications (2006) 4632–4634.
[26] Z.B. Zhuang, Q. Peng, J.F. Liu, X. Wang, Y.D. Li, Inorganic Chemistry 46 (2007) 5179–5187.
[27] H.L. Zhu, K.H. Yao, H. Zhang, D.R. Yang, Journal of Physical Chemistry B 109 (2005) 20676–20679.
[28] L.Y. Chen, X.C. Ma, Y.K. Liu, Y.G. Zhang, W.Z. Wang, Y. Liang, Z.D. Zhang, European Journal of Inorganic Chemistry (2007) 4508–4513.
[29] B. Herreros, T.L. Barr, J. Klinowski, Journal of Physical Chemistry 98 (1994) 738–741.
[30] S. Arora, M.L. Singla, P. Kapoor, Materials Chemistry and Physics 114 (2009) 107–122.
[31] L.A. Perez-Maqueda, L.F. Wang, E. Matijevic, Langmuir 14 (1998) 4397–4401.
[32] Q. Zhang, S.-J. Liu, S.-H. Yu, Journal of Materials Chemistry 19 (2009) 191–207.
[33] M.S. Lehmann, F.K. Laesen, F.R. Poulsen, A.N. Christensen, S.E. Rasmussen, Acta Chemica Scandinavica 24 (1970) 1662–1670.
[34] A.N. Christensen, R. Gronbaek, S.E. Rasmussen, Acta Chemica Scandinavica 18 (1964) 1261–1266.
[35] I. Bakó, T. Grósz, G. Pálinkás, M.C. Bellissent-Funel, The Journal of Chemical Physics 118 (2003) 3215–3221.
[36] M.F. Casula, Y.-W. Jun, D.J. Zaziski, E.M. Chan, A. Corrias, A.P. Alivisatos, Journal of the American Chemical Society 128 (2006) 1675.
[37] S.P. Harimkar, N.B. Dahotre, Journal of Applied Physics 100 (2006) 024901.
[38] H.G. Yang, C.H. Sun, S.Z. Qiao, J. Zou, G. Liu, S.C. Smith, H.M. Cheng, G.Q. Lu, Nature 453 (2008) 638–642.